# TA/TGP/13-15 - Assessing the potential of depleted gasfields for geothermal energy

29 Augustus 2013 Max Daarnhouwer

| | | |
|---|---|---|
| Title | : | Assessing the potential of depleted gasfields for geothermal energy |
| BSc thesis | : | TA 3009-10 |
| Author(s) | : | Max F. Daarnhouwer |
| Student number | : | 1340018 |
| Date | : | 29 August 2013 |
| Supervisor(s) | : | Hamidreza Salimi & Karl-Heinz Wolf |
| TA Report number | : | BTA/TGP/13-15 |
| Postal Address | : | Section for Petroleum Engineering<br>Department of Geoscience & Engineering<br>Delft University of Technology<br>P.O. Box 5028<br>The Netherlands |
| Telephone | : | (31) 15 2781328 (secretary) |
| Telefax | : | (31) 15 2781189 |

# 1 Preface

This thesis was written to finalize the bachelor program of Applied Earth Sciences at Delft University of Technology. The TU Delft has been involved in the Delft Aardwarmte Project (DAP) since 2007 and therefore I got the opportunity to work on geothermal energy. In this preface I want to thank Hamidreza Salimi and Karl-Heinz Wolf for their supervision and patience with me during this project.

# 2 Abstract

In this thesis, the feasibility of a geothermal doublet in the former Barendrecht gas field is investigated. The aim of this work is to stay as closely as possible to the original well configuration. An IMPEXS model for the movement of the cold-water and thermal front is built to calculate the possible potential of the field. Wellbore heat losses and pump capacity were taken into account to evaluate the exergy (useful energy) created by the geothermal doublet.

The results obtained by the model show that the amount of injected cold-water and consequently the amount of heat extraction from the gas field is very sensitive to the permeability of the field and the viscosity of the fluid. Inclusion of heat gain from over- and under-burden in the numerical model causes the thermal front to move slower. Since the feasibility of the project is predominantly dependent on the duration of the saturation of the field, this effect will not improve the feasibility of the project.

Because only gas at a low pressure is still present in the reservoir, the field has to be saturated with cold water before production of hot water can be started. This process takes around 30 years. After that, a production rate of 5 $m^3$/hr can be established. The temperature of the production would be 69.7 °C initially and becomes 64 °C after 500 years. When taking into account a pump that uses 100 KW to pump the water out of the formation, an exergy of 200 KW can be established.

Because of the large saturation time and the limited exergy compared to other sustainable energy sources it is concluded that this project is not feasible.

# Table of contents

## List of figures

# List of Tables

# 3 Introduction

A lot of change is needed to secure the world's energy supply in the future. Scarcity of hydrocarbons, high oil prices, transportation problems and carbondioxide emissions force mankind come up with new solutions for their energy supply. Geothermal energy is a good alternative instead of fossil fuels in order to heat buildings and to run low temperature processes. The technique is already quite old, the first geothermal installation was built in Italy around 1904, but widespread utilization was delayed until after World War II. The heat continuously flowing from the Earth's interior is estimated to be equivalent to 42 million megawatts of power. Vastly greater, in fact, than the resources of coal, oil, gas, and nuclear energy combined. The source of geothermal energy, the earth's heat, is permanently available. Solar and wind energy sources, in contrast, are dependent upon a number of factors, including daily and seasonal fluctuations and weather variations. The development costs of geothermal fields on the other hand are much higher than other renewable energy sources and a significant chance of failure is present. Recently there have been troubles with unexpected hydrocarbon production at the Pijnacker geothermal plant. Considering the above mentioned and taking into account that there are many depleted or dry gas fields in the Netherlands, there might be potential to combine geothermal and hydrocarbon exploration. Another motivation for the new interest in geothermal energy is the high-energy prices. Geothermal energy can now be produced to more market conform prices than in the past.

In the projects that were already realized in the Netherlands, geothermal energy was produced from aquifers. Aquifers are earth layers that are saturated with water. Most aquifers did not have any economic value before the introduction of geothermal energy. There are quite a lot of depleted gas fields in the Netherlands which have been abandoned. Their economic value for gas production is low, but there are production facilities in place. As a feasibility study, this thesis studies the geothermal-energy potential of the Barendrecht gas field.

In this thesis, cold water is first injected into the reservoir. Because initially there is no mobile water in the reservoir, it takes some time for injected water to reach the production well. The question that needs to be addressed is what the temperature of produced water would be. A model that includes heat and mass transfer of fluid flow in porous media is developed to assess the potential of Barendrecht gas field for geothermal energy.

Modeling geothermal reservoirs is not a new field of research, actually many techniques have been described. Bodvarsson et al. (1986), published a paper explaining different types of reservoir simulation and illustrated the implementation of injection, production and multi phase flow in their paper. Because geothermal enhancement is a hot topic in the Netherlands, many feasibility studies are performed. Recently Arvid de Groot (2011) made a feasibility analysis for the Bergermeer reservoir near Heerhugowaard. The idea of combining geothermal and hydrocarbon production is not new. Denis Pone (2004) studied this topic already for hydrocarbon fields in the Gulf of Mexico.

The first step in the study is to build a one dimensional non-isothermal model of the filling stage of the process. Because an old gas reservoir is not an aquifer, still around $67*10^6$ $Nm^3$ of natural gas and no mobile water are in place. The heat is transferred from the gas and the rocks to the water. The temperature of the reservoir is about 70 °C, so the expected potential of the field is limited. After the field is completely saturated the production well can be opened and production of warm water can start. This second step will continue until the thermal front will break through in the production well. In order to calculate the potential of this construction, heat gain from other layers is included, as well as the heat loss to the wellbore.

## 3.1 The Barendrecht Gas field

The Barendrecht field is located within the Rijswijk concession in the West Netherlands Basin, approximately three kilometers southeast of the Rotterdam field. The structure consists of a simple, low relief northwest-southeast trending faulted anticline. The lithology consists of shaly sandstones. There are two proven productive intervals in the Barendrecht field: De Lier and Ijsselmonde. The De Lier Member is the main producing interval. There are two other interpreted hydrocarbon bearing intervals, namely the Holland Greensand Formation and parts of the lower Delfland Formation.

The reservoir was originally filled with gas and oil and was produced from January 2003 until January 2010. The oil is still in place, while the gas has been produced, from a pressure of 17.3 MPa to a pressure of 3 MPa. The GIIP was estimated based on a decline curve analysis in 2007 to be $260*10^6$ $Sm^3$. This estimate was made using a porosity cut off of 11.25% and a permeability cut off of 0.2 mD. In 2010 $193.5*10^6$ $Sm^3$ have been produced. That means that there is still some $66.5*10^6$ $Sm^3$ of gas in the field. The oil in the reservoir has never been produced.

The Barendrecht gas field gained fame in the last five years because of the social/ethical discussion about carbondioxide storage in this old gas field. Because of the big amount of information available, the reservoir was chosen as subject of this feasibility study on combined geothermal and hydrocarbon exploitation. The information that I used was published by Shell $CO_2$ Storage BV. In this chapter will give an outline of the properties that are important to the model.

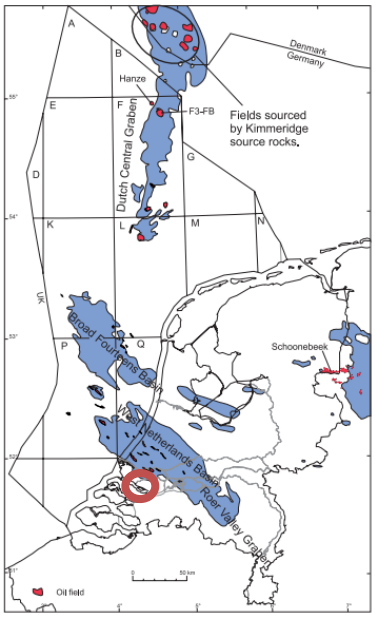


Figure 1: A map of the Dutch oil and gas basins (blue). Barendrecht is indicated with a circle.

## 3.2 Well configuration

The configuration and technical details for the two wells in the Barendrecht field was obtained using the work of Newstead (2008). BRT1 is an exploration well and is currently plugged off. In the interval of the De Lier sandstone it has a casing size of 9 5/8 inch. The other well, BRT2, had some troubles with a lost bit and is therefore sidetracked 1323 m and later also at 1502 m, resulting in the wells BRT2A and BRT2B. The first sidetrack was used for exploration purposes and from the second sidetrack the actual production happened. BRT2b was completed with a 7 inch liner. In this study well BRT 1 is used for injection, due to its larger wellbore radius

The distance between these two wells is thousand meters. The wells will not immediately be operational and will need large adaptation. Since the study is focused on combining geothermal and hydrocarbon production the use of the existing wells is preferred. Figure 2 shows the well configuration as it was designed for the hydrocarbon production.

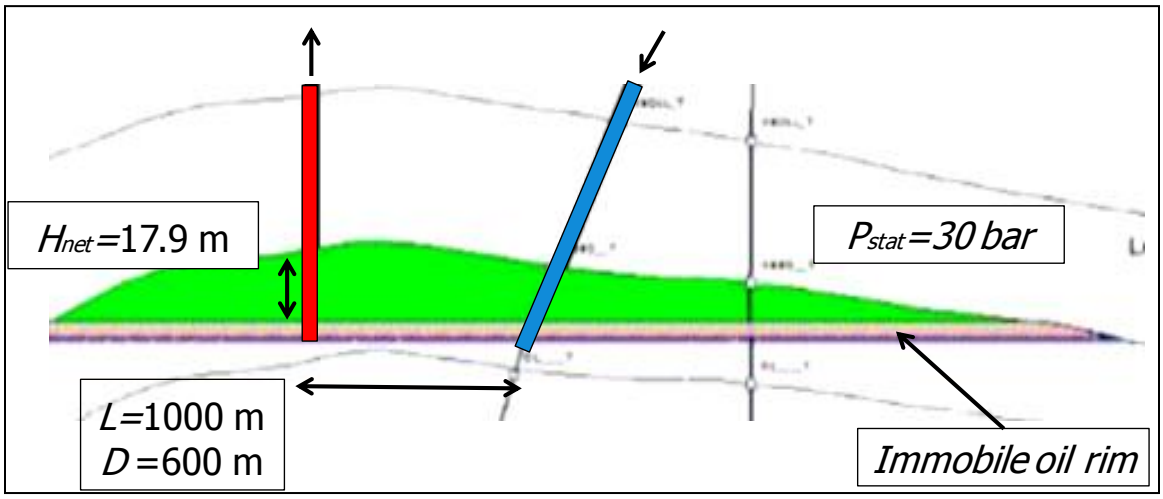


Figure 2: NW-SE Cross section of the Barendrecht field, made for CO2 storage purposes.

## 3.3 Sedimentological interpretation

This facies has a good mean porosity of 15.9 percent, though mean permeability is moderate (3.46 mD) (Dobrinsy, 2007). The grain density has a narrow range between 2.60 and 2.66 g/cm$^3$. The Argillaceous offshore facies has a porosity ranging from 5.3 to 11.6 percent, with an average of 9.1 percent. The maximum (geometric) mean permeability of this formation is 1.18 mD and is based on eight core samples, but can locally be as high as 28.9 mD. The grain density in this group is equal to that in the sandy offshore facies.

## 3.4 Reservoir quality

The De Lier Member consists of both sandy offshore and argillaceous offshore lithofacies. The sandy offshore lithofacies shows a fairly large variation in porosity and permeability, while the argillaceous lithofacies shows a narrower variation of porosity. In well BRT 1 three intervals were cored. One interval in the Middle Holland Member, one in the Greensand Member and one in the De Lier Member. At the NAM laboratories, lab-experiments were performed on these cores in order to obtain porosity and permeability values. These values are publicly available on the TNO website (NLOG.nl). In order to obtain a formula that calculates the permeability in the different layers as a function of the porosity, a least squares trend line was plotted through a cross-plot of porosity and log permeability values. In Figure 3 the porosity-permeability (*PHI-k*) crossplot of the De Lier Formation, based on plug measurements is shown. Using a least squares trendline through the cloud of points a *PHI-k* relation was obtained. This *PHI-k* relation was consecutively applied to a porosity log obtained by applying equation (1) on the density log.

$$\varphi = \frac{\rho_{mat} - \rho_{bulk}}{\rho_{mat} - \rho_{fluid}} \qquad (1)$$

In which $\varphi$ is porosity and subscripts mat, bulk and fluid indicate the density of respectively the matrix, the bulk and the fluid. For the matrix density an average matrix density of 2.63 gr/cm$^3$ was used. The density of the oil based drilling fluid was used as fluid density, namely 0.8 gr/cm$^3$.

For the interval between the top of the reservoir and the gas-oil-contact (GOC) an average reservoir permeability of 3.37 mD was obtained using a arithmetic average. This number is close to the 3.47 mD calculated in the Technical Field Development plan (Newstead J. , 2008). The log section of the calculated permeability log in well BRT-1 can be found in Appendix D - Permeability Log.

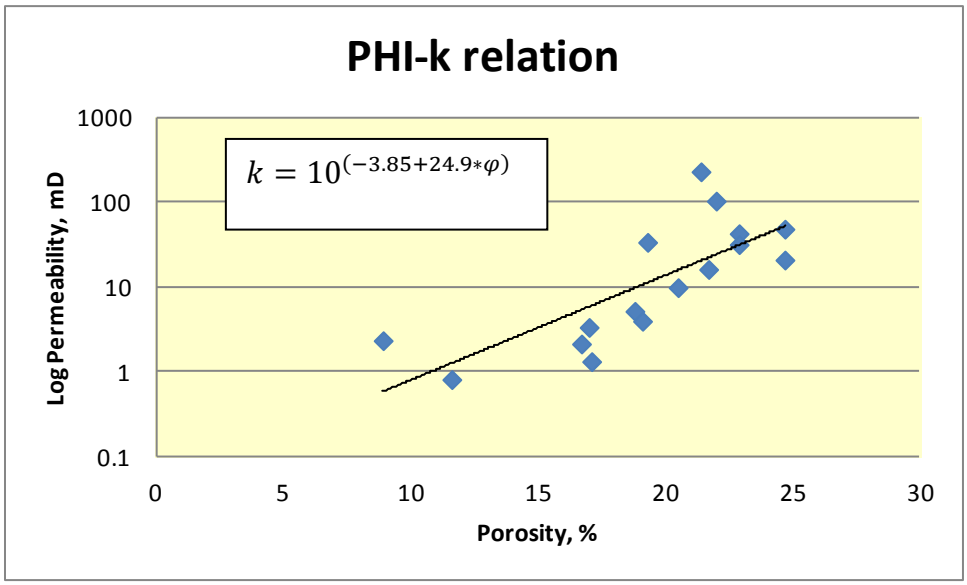


Figure 3: *PHI-k* relation based on cores from the De Lier Formation in the Barendrecht Field

# 4 Model equations for non-isothermal flow

A model in which the components, (e.g., methane and water) form at most two phases (e.g., gas and aqueous) is considered. In the model, it is assumed that the displacement is immiscible (i.e., the gaseous phase and aqueous phase do not mix with each other and phase portioning does not occur). The governing equations for non-isothermal two -phase flow are given by the mass conservation equations, Darcy's law and the energy conservation equations.

## 4.1 Two-phase equations

Let $\varphi$ and $K$ be the porosity and permeability of a geothermal reservoir. $S_\alpha$, $\rho_\alpha$, $\mu_\alpha$, $u_\alpha$, $k_{r\alpha}$ be the saturation, density, viscosity, volumetric velocity, relative permeability of the alpha-phase, $\alpha = w, g, s$ respectively. Because the permeability of the aqueous phase is influenced by the saturation of the gaseous phase, it can no longer only be described by the permeability of the rock only. Therefore the relative permeability is introduced, the relative permeability is a function of wettability and saturation of one phase for a two phase system.

## 4.2 Mass conservation equations

Mass conservation for phase alpha is given by the following equation:

$$\frac{\partial}{\partial t}(\varphi S_\alpha \rho_\alpha) + \nabla.(u_\alpha \rho_\alpha) = 0 \tag{2}$$

The total mass conservation equation reads:

$$\frac{\partial}{\partial t}\varphi\left(S_w \rho_w + S_g \rho_g\right) + \nabla.\left(u_w \rho_w + u_g \rho_g\right) = 0 \tag{3}$$

The volumetric velocity is given by Darcy's equation, with the gravity pointing downwards and can be written as follows:

$$u_\alpha = -\frac{K k_{r\alpha}}{\mu_\alpha} K(\nabla P - \rho g) \tag{4}$$

In this model it is assumed that there is no gravity, so the gravity term in the Darcy equation (4) turns zero, resulting in the following equation:

$$u_\alpha = -\frac{K k_{r\alpha}}{\mu_\alpha} \mathrm{K}\nabla P \tag{5}$$

We introduce the phase mobility as follows

$$\lambda_\alpha = \frac{K k_{r\alpha}}{\mu_a} \tag{6}$$

If capillary pressure is disregarded, the phase pressure gradient in equation (5), becomes the same for both the gaseous phase and aqueous phase. Consequently, the ratio between the phase volumetric velocities becomes the same as the ratio between the phases mobilities, i.e.,

$$u_\alpha = \frac{u_w}{\lambda_w}\lambda_g \tag{7}$$

Substituting equations (3), (5) and (7) give the following equation for the mass balance. The pores are occupied either by water or by gas, so $S_g = 1 - S_w$ .

$$\frac{\partial}{\partial t}\varphi\left(S_w\rho_w + (1-S_w)\rho_g\right) + \nabla.\left(u_w\rho_w + \frac{u_w}{\lambda_w}\lambda_g\rho_g\right) = 0 \tag{8}$$

## 4.3 Heat conservation equation

With equations (2) until (8) it is possible to simulate the fluid flow in the reservoir. The next step is to find an equation for the heat conservation in the reservoir. The heat conservation balance is given by

$$\frac{\partial}{\partial t}\left[\varphi\left(S_w H_w\rho_w + S_g H_g\rho_g\right) + (1-\varphi)H_s\rho_s\right] + \nabla.\left(u_w H_w\rho_w + u_g H_g\rho_g\right) = 0 \tag{9}$$

The first term gives the internal energy in the liquid, the second term gives the internal energy in the gas, the third term gives the internal energy in the solid, the fourth term gives the net flow of heat by convection, and the fifth term gives the net heat flow by conduction.

In this model, it is assumed that the net heat flow by conduction can be neglected and is therefore be equal to zero. It is further assumed that the enthalpies are equal to the internal energies of the different phases, this makes it easier to deal with the changing pressures and volumes. The next equation shows this assumption, with $H_\alpha$ for the specific enthalpy of phase alpha, $c_\alpha$ is the specific heat capacity of phase alpha and $T$ the temperature.

$$H_\alpha = C_{p\alpha}T \tag{10}$$

Having taken all these assumptions into account, we end with the following equation for heat conservation

$$\frac{\partial}{\partial t}\left[\varphi\left(S_w c_{p,w}\rho_w T + S_g c_{p,g}\rho_g T\right) + (1-\varphi)c_s\rho_{p,s}T\right] + \nabla.T\left(u_w c_{p,w}\rho_w + u_g c_{p,g}\rho_g\right) - \nabla.\lambda\nabla = 0 \tag{11}$$

# 5 Model Parameters

## 5.1 Viscosity

### 5.1.1 Water viscosity

The viscosities of the liquid phase are approximated by the viscosities of water as a function of temperature and pressure (Perry and Green 1997)

$$\mu_w = 2.414 * 10^{-5} * 10^{(247.8/(T-140)} \tag{12}$$

### 5.1.2 Gas viscosity

For the gas viscosity, a graphical correlation by Carr, Kobayashi and Burrows (1954) was used. A numerical approximation of this correlation was given by Dempsey (1965) and can be written as follows:

$$\mu_g = f(p_{pr}, T_{pr}) * \mu_{g,p_{g,sc}}(M, T) \tag{13}$$

where *f* is a function of the pseudo reduced pressure and pseudo reduced temperature. The function of this equations is to transform the viscosity from the standard pressure to a viscosity at the desired conditions. The pseudo reduced pressure ($p_{pr}$) and temperature ($T_{pr}$) can be found as follows:

$$p_{pr} = \frac{p}{p_{pc}} = {}^{p}/_{(5218 * 10^3 - 734 * 10^3 * \rho_{g,sc} - 16.4 * 10^3 {\rho_{g,sc}}^2)} \tag{14}$$

$$T_{pr} = \frac{T}{T_{pc}} = {}^{T}/_{(94.0 + 157.9\rho_{g,sc} - 27.2{\rho_{g,sc}}^2)} \tag{15}$$

The next step is to calculate the *f*-function:

$$\begin{aligned} f = \frac{1}{T_{pr}} EXP\big[a_0 + a_1 p_{pr} + a_2 p_{pr}^2 + a_3 p_{pr}^3 + T_{pr}\big(a_4 + a_5 p_{pr} + a_6 p_{pr}^2 + a_7 p_{pr}^3\big) \\ + T_{pr}^2\big(a_8 + a_9 p_{pr} + a_{10} p_{pr}^2 + a_{11} p_{pr}^3\big) + T_{pr}^3(a_{12} + a_{13} p_{pr} \\ + a_{14} p_{pr}^2 + a_{15} p_{pr}^3)\big] \end{aligned} \tag{16}$$

$$\mu_{g,p_{sc}} = b_0 + b_1 T + b_2 T^2 + b_3 M + b_4 TM + b_5 T^2 + b_6 M^2 + b_7 TM^2 + b_8 T^2 M^2 \tag{17}$$

The dimensionless coefficients for *a* and *b* are given in Table 1. In equation (17), *M* and *T* are the molecular weight and the absolute temperature.

| Table 11: Carr Kobayashi and Burrows (1954) coefficients for gas viscosity calculation. Coefficients for gas viscosity functions | | | |
|---|---|---|---|
| **a0** | -2.4621182E+00 | **b0** | 1.1123191E-05 |
| **a1** | 2.9705471E+00 | **b1** | 3.0190789E-08 |
| **a2** | -2.8626405E-01 | **b2** | 6.8480801E-12 |
| **a3** | 8.0542052E-03 | **b3** | -1.0948505E-07 |
| **a4** | 2.8086095E+00 | **b4** | -1.1525695E-10 |
| **a5** | -3.4980331E+00 | **b5** | -2.9139735E-13 |
| **a6** | 3.6037302E-01 | **b6** | 4.5773519E-10 |
| **a7** | -1.0443241E-02 | **b7** | 3.8322610E-13 |
| **a8** | -7.9338568E-01 | **b8** | 1.2886525E-15 |
| **a9** | 1.3964331E+00 | | |
| **a10** | -1.4914493E-01 | | |
| **a11** | 4.4101551E-03 | | |
| **a12** | 8.3938718E-02 | | |
| **a13** | -1.8640885E-01 | | |
| **a14** | 2.0336788E-02 | | |
| **a15** | -6.0957926E-04 | | |

## 5.2 Density

### 5.2.1 Water density

In the model, the water temperature varies from 20 °C at the injector to 72 °C at the producer. The pressure varies from atmospheric to 30 Mpa. To adapt the density of the water to the changing condition the understanding equation was used, in which $p_0$, $T_0$ and $\rho_0$ are the injection pressure, temperature, and density, $E$ and $\beta$ are the bulk modulus and volumetric temperature coefficient. $E$ is assumed to be equal to $2.2\times10^9$ Pa and $\beta$ is equal to $207*10^{-6}$ $K^{-1}$.

$$\rho_w = \left(\frac{\rho_0}{(1+\beta(T_1-T_0)}\right) \Big/ \left(\frac{1-(p_1-p_{0)}}{E}\right) \tag{18}$$

### 5.2.2 Gas Density

The gas in the reservoir consists of a mixture of different types of hydrocarbon gasses, nitrogen, carbon dioxide and a very small amount of hydrogen sulfide. In the model an estimated equation for the Standing and Katz $Z$-factor was used. This equation is called the Beggs and Brill (1973) correlation and was designed to calculate the compressibility of gas in multiphase flow lines, and is essentially a best-fit equation to the standard Standing and Katz $Z$-factor chart. This $Z$-factor describes how much the gas deviates from the ideal gas law, as a function of pseudo reduced pressure and temperature and can be inserted in the ideal gas law as follows:

$$\rho_g = \frac{Mp}{ZRT} \tag{19}$$

Where $M$ is the molecular weight of the gas. In order to calculate the pseudo reduced pressure and temperature the relative density is needed. The composition of the gas is known and can be used to calculate the relative density from the gas to air.

Table 2: Gas Composition. (van Bergen, 2007)

| Gas Compostion "De Lier Member", BRT1 | | | |
|---|---|---|---|
| | **av. mol%** | **M, g/mol** | **Weight, g** |
| $C_1$ | 87.5 | 16.04 | 14.04 |
| $C_2$ | 5.55 | 30.07 | 1.67 |
| $C_3$ | 1.85 | 44.10 | 0.82 |
| $C_4$ | 1.15 | 58.12 | 0.67 |
| $C_5$ | 2.15 | 72.15 | 1.55 |
| $C_6$ | 0.05 | 86.17 | 0.04 |
| $n_2$ | 1.45 | 28.01 | 0.41 |
| $CO_2$ | 0.32 | 44.01 | 0.14 |
| | | | |
| Total weight of gas | | | 19.33 |
| Relative density | | | 0.67 |

To make the Beggs and Brill (1954) correlation a little better understandable. the equation was separated in different parts. The pseudo-reduced pressure and temperature are calculated in equations (14) and (15).

$$Z = A + \frac{(1-A)}{e^B} + CP_{pr} \tag{20}$$

$$A = 1.39(T_{pr} - 0.92)^{0.5} - 0.36T_{pr} - 0.101 \tag{21}$$

$$B = \left(0.62 - 0.23T_{pr}\right)P_{pr} + \left(\frac{0.066}{\left(T_{pr} - 0.86\right)} - 0.037\right)P_{pr}^2 + \frac{0.32}{10^{9(T_{pr}-1)}}P_{pr}^2 \tag{22}$$

$$C = \left(0.132 - 0.32\log\left(T_{pr}\right)\right) \tag{23}$$

$$D = 10^{\left(0.3016 - 0.49T_{pr} + 0.1824T_{pr}^2\right)} \tag{24}$$

With the Z-factor and all the other components of the ideal gas law known, the gas density can now be determined.

## 5.3 Heat capacity

Both heat capacity functions were derived with the help of a trend line through tabulated values.Tabulated values were obtained from (Engineeringtoolbox.com, Methane Specific Heat, 2011) and (Engineeringtoolbox.com, Water-Thermal Properties, 2011)

$$cp_w = 0.0103T^2 - 6.3608T + 5164.3 \tag{25}$$

$$cp_g = 1000(0.0026T^2 + 1.4701) \tag{26}$$

## 5.4 Relative permeability

The mobility of a phase is a property that is used to describe the ease of a fluid to migrate through a porous medium in the presence of another fluid. In this model the following formulas were used to calculate the mobility.

$$\lambda_{rw} = \frac{K k_{rw} S_e^{nw}}{\mu_w} \tag{27}$$

$$\lambda_{rg} = \frac{K k_{rg} (1 - S_e)^2 (1 - S_e^{n0})}{\mu_g} \tag{28}$$

$$\text{Total mobility} = \lambda_{tot} = \lambda_{rw} + \lambda_{rg} \tag{29}$$

In these equations k, $k_{rw}$, $k_{rg}$, $S_e$, $\mu_w$, $\mu_g$ are respectively standing for permeability, relative permeability of water, relative permeability of gas, saturation, viscosity of water and viscosity of gas. The values for relative permeability of water and gas are calculated with the Brooks and Corey (1964) equations:

$$k_{rw} = (1 - S_g)^{\frac{2+3\lambda}{\lambda}} \tag{30}$$

$$k_{rg} = S_g^2 (1 - (1 - S_g)^{\frac{2+\lambda}{\lambda}} \tag{31}$$

Where $\lambda$ is the sorting factor. Typical values for $\lambda$ are $0.2 < \lambda < 7$. A value of $\lambda = 2$ is used in this numerical model.

## 5.5 Fractional flow and flow rate

In the model we need to define the flow rate at different locations in the reservoir in order to calculate the water saturation. If the water is injected, a two-phase system with water and gas is developed.

$$u_w = f_w u_t \; and \; u_g = f_g u_t \tag{32}$$

$$u_t = u_w + u_g \tag{33}$$

where $f_w$ and $f_g$ are the water and gas fractional-flow function and $u_t$ is the total velocity. The flow rates of the different phases can be replaced by Darcy`s Law.

$$u_t = -\lambda_w \left( \frac{\partial p_w}{\partial x} + \rho_w g \frac{\partial z}{\partial x} \right) - \lambda_g \left( \frac{\partial p_g}{\partial x} + \rho_g g \frac{\partial z}{\partial x} \right) \tag{34}$$

$$u_t = -(\lambda_w + \lambda_g) \left( \frac{\partial p_w}{\partial x} + \rho_w g \frac{\partial z}{\partial x} \right) - \lambda_g \left( \frac{\partial}{\partial x} (p_g - p_w) + (\rho_g - \rho_w) g \frac{\partial z}{\partial x} \right) \tag{35}$$

$$u_t = \left( \frac{\lambda_w + \lambda_g}{\lambda_w} \right) u_w - \lambda_g \frac{\partial p_c}{\partial x} + \lambda_g \Delta \rho_{wg} g \frac{\partial z}{\partial x} \tag{36}$$

$$u_w = \frac{\lambda_w}{\lambda_w + \lambda_g}\left[u_t + \lambda_g \frac{\partial p_c}{\partial x} - \lambda_g \, \Delta\rho_{wg} g \frac{\partial z}{\partial x}\right] \tag{37}$$

In the model a horizontal reservoir with no capillary forces was assumed. Because of these assumptions, the third and fourth term on the right hand side of the equation becomes equal to zero. The equation for fractional flow of water or gas becomes quite simple now.

$$u_w = \frac{\lambda_w}{\lambda_w + \lambda_g} u_t, \text{ so } f_w = \frac{\lambda_w}{\lambda_w + \lambda_g} \tag{38}$$

In a similar manner, fractional gas flow can be found:

$$f_g = \frac{\lambda_g}{\lambda_w + \lambda_g} \tag{39}$$

In the model the fractional flow theory was used to find the flow rate. Because this model is dealing with a geothermal reservoir, in which temperatures are not constant, it has to be taken into account that densities of different reservoir fluids can change. Based on the fractional flow and the density in the cell at the previous time, the flow rate in the cell at the current location can be calculated. The densities at the current location are based on initial values, which are subsequently updated through iteration. The formula looks as follows:

$$u_{tot,i} = u_{tot,i-1}\left(\frac{\rho_{w,i-1}}{\rho_{w,i}} f_{w,i-1} + \frac{\rho_{g,i-1}}{\rho_{g,i}} f_{g,i-1}\right) \tag{40}$$

The flow rate in the first cell, that is from the wellbore into the field, is dependent on the pressure difference between the wellbore and the field. To determine a suitable flow rate for this cell the following injectivity equation was used:

$$u_{tot,1} = \frac{2\pi(\lambda_{rw} + \lambda_{rw})(p_{wf} - p)}{\log\left(0.208 \frac{dz}{r_w}\right) w} \tag{41}$$

## 5.6 Water saturation

From equation (40) the flow rate at every location in the reservoir can be calculated. The flow rate can now be used to solve the following differential equation for the saturation:

$$\frac{\partial(\varphi S_w \rho_w)}{\partial t} + \frac{u_t}{\varphi}\frac{\partial \rho_w f_w}{\partial x} = 0 \tag{42}$$

$$\partial S_w = \frac{(\rho_{w,i-1} f_{w,i-1} u_{t,i-1} - \rho_{w,i} f_{w,i} u_{t,i})}{\rho_{w,i} \varphi dz} \Delta t \tag{43}$$

The porosity is assumed constant for the entire reservoir, flow rate and fractional flow are also known for the entire reservoir for every time. In the model $\partial S_w$ is added to the initial water saturation. The numerical calculation is shown in the appendix A.

## 5.7 Temperature profile

The numerical derivation for the temperature profile can be found in appendix A.

## 5.8 Pressure

The De Lier Formation has a very low permeability for water flow. According to the Darcy equation, we know that a fluid needs a high pressure to flow through a low permeability matrix. It turned out that injection pressures far above the maximum pressure that the reservoir rock can withstand were necessary. It was decided to make the flow rate dependent on a maximum pressure difference in the field. The bottomhole pressure was fixed at a maximum value of 20 MPa and the flow rate was adjusted to this maximum pressure. To introduce a maximum pressure difference over the field, the injection rate has to be variable. In the model this was achieved by the use of the IMPEXS numerical scheme. IMPEXS is an abbreviation for implicit pressure and explicit saturation. The code which has been used can be found in Appendix C.

## 5.9 Time

To solve the saturation profile a stable time step is needed at all times. In the beginning these time steps will be quite small, while the time step will increase when more water gets injected. For the first four iterations of the model a time step of $1*10^{-4}$ seconds is allowed. When the number of iterations is above four, the following formula is used:

$$dt^n = \min\left(dt^{n-1}\left(\frac{dsmax}{maxds}\right)^{0,1}; 0.2\frac{dz}{u_{tot}}\right) \tag{44}$$

where *dsmax* is the maximum allowed change in saturation per time step, maxds is the maximum observed saturation change per time step, $u_{tot}$ is the interstitial velocity at the maximum flow rate and *dz* is the grid size.

# 6 Results of the model and discussion

The whole modeling process resulted in a one-dimensional model for the Barendrecht Field. Because of the limited amount of time available and the complexity of the thesis, it was assumed that the reservoir has a constant permeability equal to the arithmetic average of the De Lier interval (3.5 mD) No heterogeneities or other complex geometries were taken into account. The model gives results for a reservoir of 1000 meters long and 600 meters deep and 12 meters high. Because the model runs on average values, it can easily be adapted to assess the geothermal potential of other gas fields with a low permeability. In Appendix C all the input variables of the model as we used are listed.

## 6.1 Sensitivity analysis

Not every parameter has the same effect on the accuracy of the model. In this chapter the effect of the different parameters on the model results is evaluated. The method used in to investigate the influence of different parameters is relatively simple. The model is being run several times with different parameters kept constant. Parameters that are used in this test are density, viscosity and heat capacity. When it turns out that these parameters have a small influence on the results, we can decide to keep them constant. In this way, we can enhance computational efficiency. An overview of the influence of the different sensitivities on the model can be found in Table 3.

Table 3: Time needed to fully saturate the reservoir plus the time needed until breakthrough occurs .

| Model | time, yr. | position heat front, m |
|---|---|---|
| Original | 31.9 | 450 |
| $\rho_w$ = 990 $kg/m^3$ | 30.3 | 430 |
| $\rho_g$ = 65 $kg/m^3$ | 29.5 | 460 |
| Cpw = 4180 $^{J}/_{kg*K}$ | 31.7 | 410 |
| Cpg = 2232 $^{J}/_{kg*K}$ | 29.9 | 420 |
| $\mu_w$ = 0.001 Pa*s | 50.0 | 460 |
| $\mu_g$ = 0.4e-4 Pa*s | 31.5 | 430 |

### 6.1.1 Constant Viscosity Model

A first look on the model shows big differences in the spreadsheet for the water viscosity values. The values vary from $10^{-3}$ to $0.4 * 10^{-4}$ Pa*s at different temperatures and pressures. In the figure the saturation- and corresponding temperature profile are plotted. A value of $10^{-3}$ Pa*s was used in the constant viscosity model.

In Figure 4 it can be seen that the water migrates at higher velocity through the reservoir. With the variable viscosity, the reservoir is fully saturated in 32 years instead of 50 years. The varying viscosity values are used in the formula for relative permeability. So a lower value for viscosity gives a higher mobility and also a higher flow rate (equations (27) and (37)). A variable viscosity for water should absolutely be implemented when reservoir models are made. Lower values of viscosity can speed up the process significantly and are therefore crucial to in making accurate predictions. From Figure 4 it can also be seen that the temperature front also makes significantly more progress in the case of variable viscosity values.

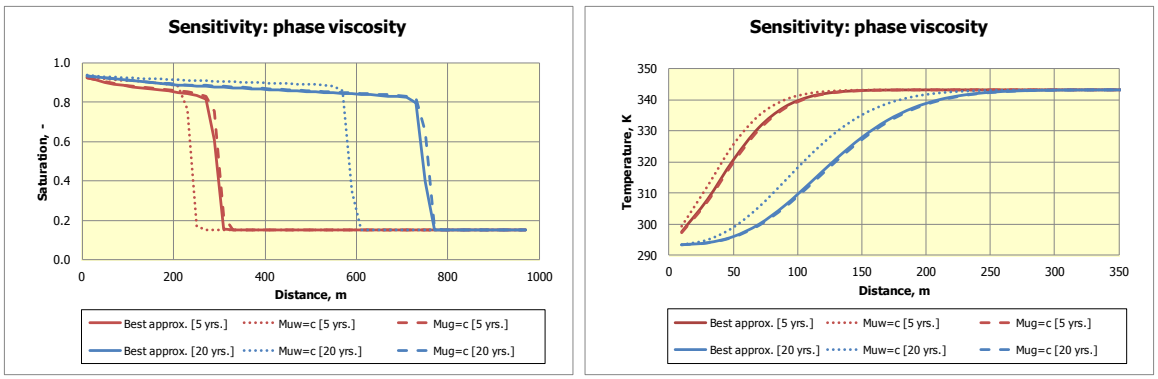


Figure 4: Sensitivity on viscosity; position of the saturation front (left) and position of the temperature front (right).

### 6.1.2 Constant density model

The model was also modified for a constant gas density. Due to the variable pressure, the density of the gas during this process increases from 21 kg/m$^3$ to 140 . kg/m$^3$. The average value over the process at the end situation was used to run the model for a constant density ($\rho_g$ =65 kg/m$^3$). If there is such a large range of input values it can be expected that the differences with the original outcome are quite large.

From equation (40) it can be seen that the total flow rate is influenced by the ratio of the current and the previous density. A lower value of gas density will make it easier for water to flow through the reservoir. With a constant density of 65 kg/m$^3$ a higher flow rate can be achieved. Because this constant density causes such big deviations from the real situation, it is not advisable to make the density constant.

For water there is a totally different situation. The compressibility of water is much lower than that of gas, so the range of densities will be much smaller. Running the model for a density of 990 kg/m$^3$ did not give significantly different values from the original situation.

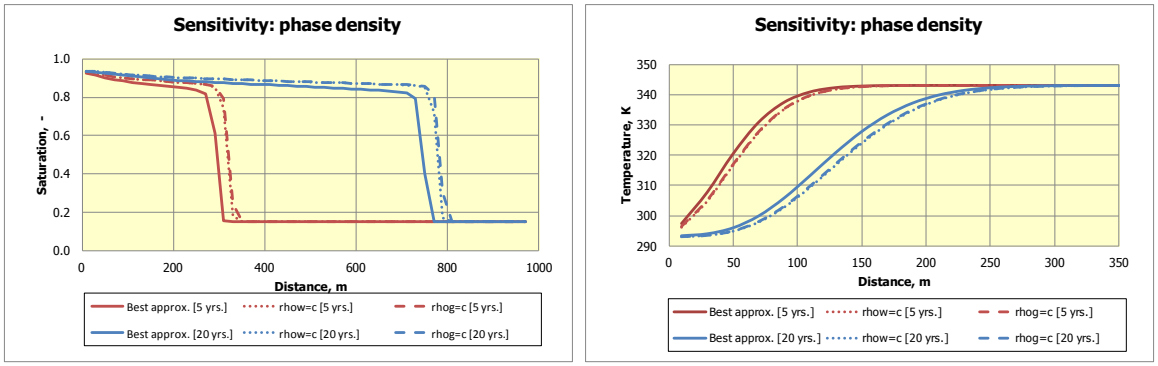


Figure 5: Sensitivity on density; position of the saturation front (left) and position of the temperature front (right).

### 6.1.3 Constant heat capacity model

The fluctuations in the heat capacity of water caused by differences in temperatures are small, so when keeping them constant will only give insignificant errors in the system. However the heat capacity of gas has a larger influence on the results of the model. The heat capacity influences the calculated temperature in the model and thereby the viscosity of the fluids. In the sensitivity, both the heat capacities for water and gas were higher than in the best guess model, causing a shorter saturation time.

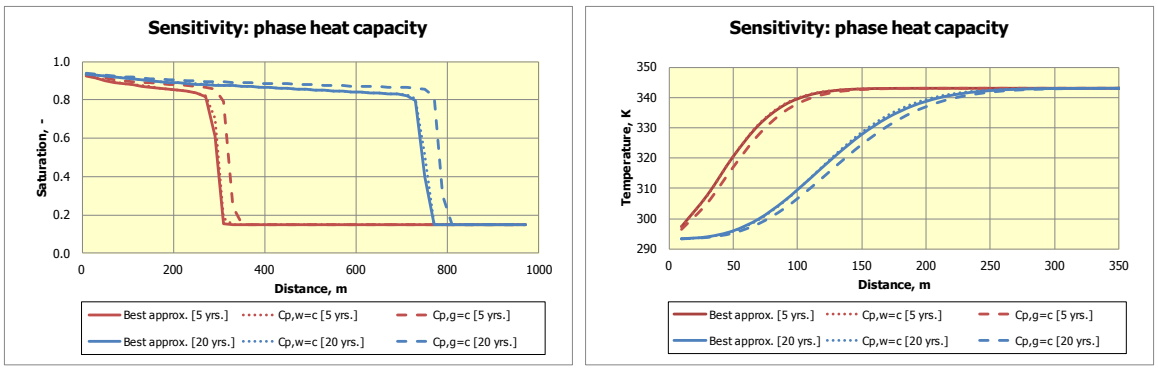


Figure 6: Sensitivity on heat capacity; position of the heat front (left) and position of the temperature front (right).

### 6.1.4 Permeability variation

The permeability has a very large control on the velocity of the saturation front. In case of a higher permeability, more water can be injected below the pressure criterion. The water also moves more easily through the reservoir. Figure 7 shows the difference in the position of the water front for the best approximation compared to cases with permeabilities of 10 mD and 100 mD.

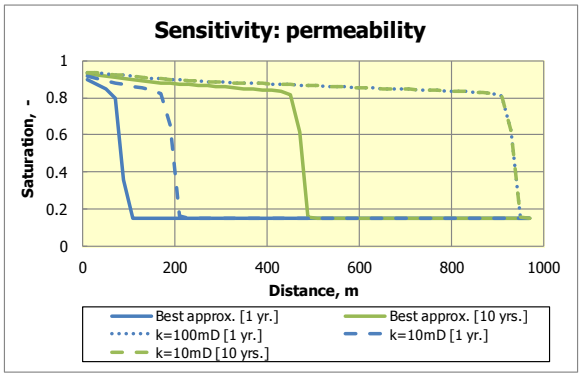


Figure 7: Sensitivity on permeability

### 6.1.5 Best approximation

This model should be the best approximation of the real situation. All parameters in the model are variable with respect to temperature and pressure. In Figure 8 the different saturations over 32 years are plotted. Because of the increase in reservoir pressure, the injection rate reduces over time. This can easily be seen in Figure 8, because the difference between the saturation lines for the same time interval becomes smaller. This effect is amplified by the increasing resistance of the compressed gas.Another interesting result is the decline in the saturation profile at full saturation (indicated as saturation after 30 years in Figure 8). Before injection of water, the reservoir was saturated by natural gas at 30 MPa. With increasing water saturation and immiscible state, the gas was first pushed forward in the reservoir while it is compressed. The decline in the blue line was caused by these two events.

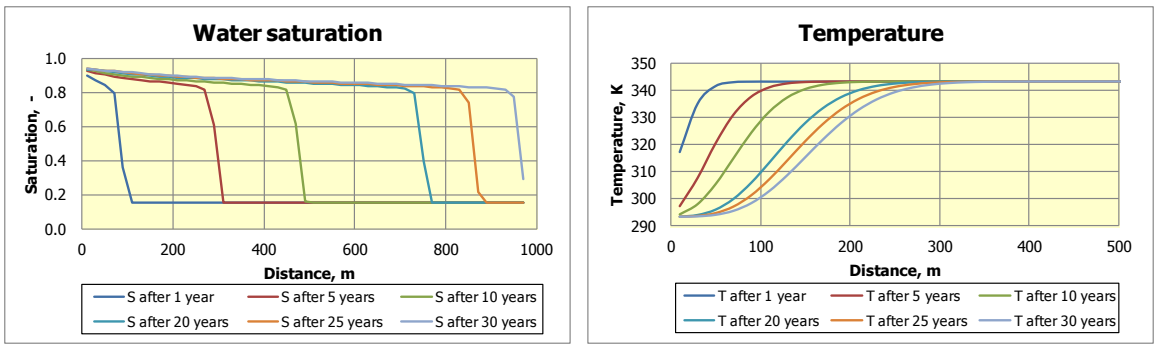


Figure 8: Saturation and heat front profiles for the best approximation case

## 6.2 Injection rate

The injection rate of the model is variable and is adapted to the maximum pressure that the rock can withstand. The maximum bottomhole pressure is set to 20 MPa. The injection rate was calculated with the use of the following injectivity equation:

$$q_{inj} = \frac{2\pi(\lambda_{rw} + \lambda_{rg})}{LOG\left(0.208\frac{dz}{r_w}\right)}(p_{wf} - p_1) \tag{45}$$

In this equation dz is the size of one gridblock and $p_1$ is the pressure in the first gridblock, which is calculated by the numerical IMPEXS scheme. From this equation it can be seen that an increase of pressure in the wellbore will increase the injection rate. If the injection continues the higher pressure that is present in the borehole will propagate into the reservoir and cause the pressure in the first gridblock to rise. When the difference between reservoir pressure and borehole pressure is decreased the injection rate will drop as a result. This effect is shown graphically in Figure 10. In Figure 9 the pressure profile caused by the injection of water into the reservoir is shown. On this picture it can be seen that the pressure around the injection well is increased a lot, while the pressure at the production well (distance = 1000 m.) only changes at the time that the reservoir is fully saturated.

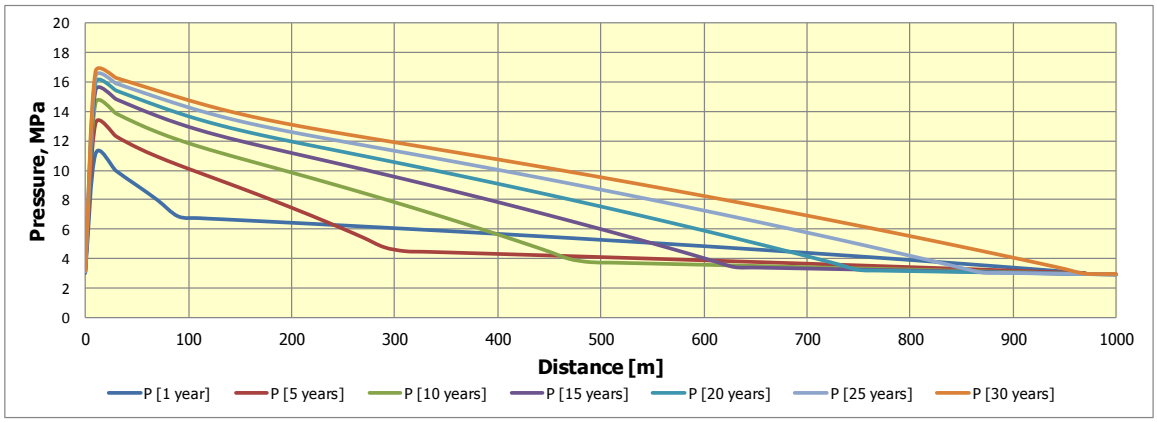


Figure 9: Pressure profile in the reservoir at different times

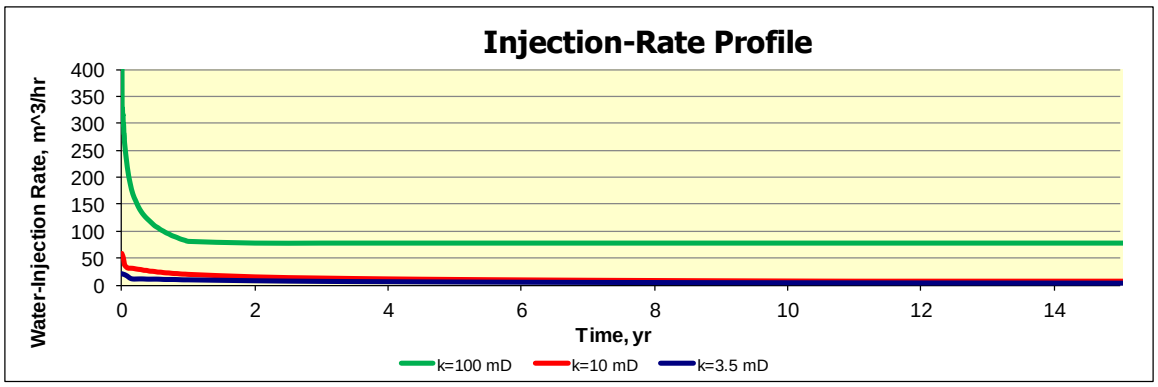


Figure 10: Maximum water injection rate over time

## 6.3 Heat gain from other layers

The reason that the subsurface contains more heat than the surface lies deep in the centre of the earth. The heat in the core of the earth is generated by nuclear reaction and is slowly transferred to the surface by convection streams of magma and by conduction through the crust. The temperature difference caused by the conduction of heat is called the geothermal gradient. The geothermal gradient at our well location is approximately 3.24°C/100 m. (van Bergen, 2007) This same gradient is also present in our reservoir, so during the geothermal enhancement process the upper and lower frontiers of the reservoir keep the initial temperature. At least this is what we assumed in the first model. The second version of the model contains a heat gain term, which assumes that the temperature difference caused by the process is reduced by conduction of heat from the upper and lower layers. The heat equation of this model looks as follows (Salimi, 2010):

$$\Delta Q = \frac{k_{ts}\Delta T}{\sqrt{\pi\alpha_{ts}(t-t_k)}}, \text{ with } \alpha = \frac{k_{ts}}{\rho c_p} \tag{46}$$

With $\Delta Q$, $k_{ts}, \Delta T, \alpha_{ts}$ $t_k$, representing respectively energy difference $[J/m^3]$, conductivity $[W/mK]$, temperature difference $[K]$, diffusivity $[m^2/s]$ and time [s] at which the temperature difference first occurred. In this model a value of 2.42 (conductivity of sandstone) was used for $k_{ts}$. Implementing this heat gain term in the total heat balance gives:

$$\frac{1}{\Delta t}[\varphi(S_w c_{p,w} T\rho_w + S_g c_{p,g} T\rho_g) + ((1-\varphi)c_{p,s} T\rho_s)] + \frac{1}{\Delta x}\varphi[u_w\rho_w c_{p,w} T + u_g\rho_g c_{p,g} T + 2\Delta Q] = 0 \tag{47}$$

Implementing this term has a big influence on the shape of the temperature front. In Figure 11 a model with and without heat gain term are plotted together. In models with a low injection rate and long injection times, this factor can have a large influence on the durability of the reservoir. It should be mentioned that the thickness of the reservoir determines the effect of the heat gain term. The reservoir in this study is relatively thick, but thinner layers will be much more sensitive to the heat gain term. In some cases the term can even delay the breakthrough of the thermal front.

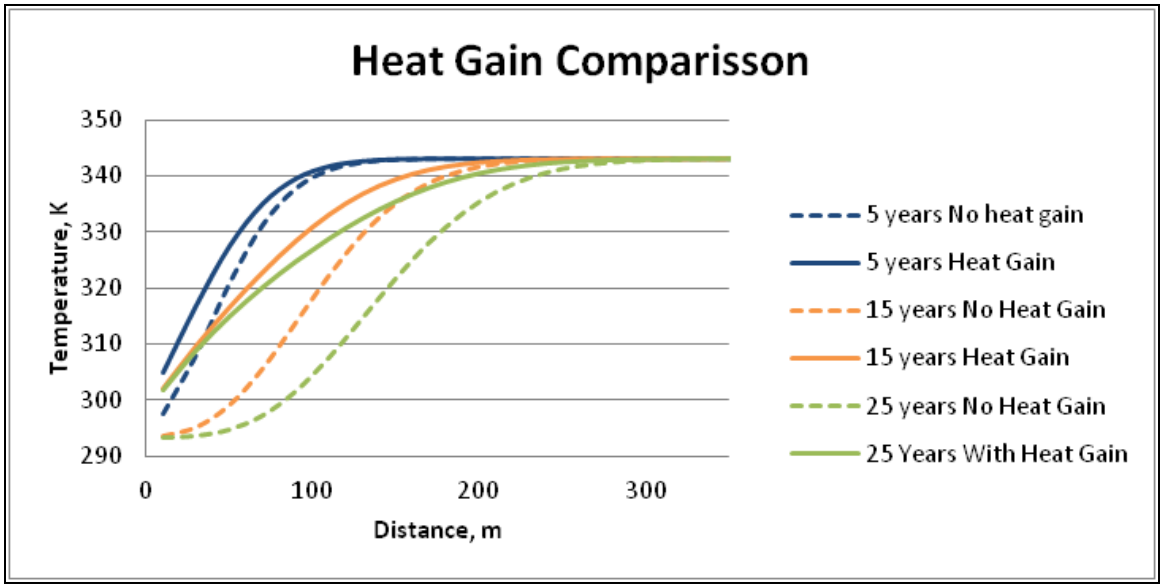


Figure 11: Temperature front with and without heat gain

## 6.4 Exergy

In the previous chapters we have seen that heat can be extracted from the reservoir at a restricted rate. In this part of the results exergy (useful energy) calculations will be made to show whether the geothermal project produces any positive useful energy. The only source of heat production is the water that is being produced from the field. A lot of energy is needed to keep the process going. In this calculation the injection resistance, the pipe resistance and the energy needed to pump up the water are included. It is also assumed that all the energy that is extracted from the reservoir can be used usefully.

### 6.4.1 Energy dissipation in the tubing

To make a fluid flow through a pipe, a certain amount of energy is lost due to frictional forces. The frictional forces will cause a decrease in pressure, which in most cases should be compensated by extra pump capacity. With the use of the fanning friction factor the pressure drop over the tubing can be calculated as follows:

$$f = \frac{D}{4L}\frac{\Delta\Phi}{\frac{1}{2}\rho v^2} \tag{48}$$

$f$ can be found after calculation of the Reynolds number. The injection rate is equal to 5 $m^3/hr$, which is 0.0014 $m^3/s$. The diameter of the wellbore is 0.10 m, so the velocity is $0.0014\ /(\pi * 0.05^2) = 0.178\ m/s$. This results in a Reynolds number of 17800 and from the Moody diagram for a relative roughness of 0.1 a value of 0.05 is found for *f*. Now equation 48 can be solved and gives a pressure drop of $1.5*10^4$ Pa. The same roughness and flow rates are assumed for both injection and production well.

$$Dissipation = \Delta\Phi * \mathrm{Q} = 1.5 * 10^4 * (5/3600) = 0.02\ \mathrm{KW} \tag{49}$$

### 6.4.2 Power loss in the reservoir

Injection of water into the reservoir is obtained due to the hydrostatical pressure, so no extra pumps are required. On the production side some artificial lift will be necessary, because the

bottomhole pressure is below the hydrostatic pressure of the formation. In order to maintain sufficient reservoir pressure, the field production is assumed to be equal to the field injection. From the model it turned out that a bottomhole pressure (BHP) of 1.4 MPa is required in order to produce the desired 5 $m^3/hr$.

$$\Delta P = (\rho g z + P_{atm}) - BHP = 9.81 * 1925 * 1000 + P_{atm} - 1.4 * 10^6 = 17.6\ MPa \quad (50)$$

This means that an extra 17.6 MPa should be overcome to achieve the desired bottomhole pressure.

$$Dissipation = \Delta\Phi * \mathrm{Q} = 17.6 * 10^6 * (5/3600) = 24.4\ \mathrm{KW} \quad (51)$$

Taking into account that the efficiency of such pumps with low flow rates is usually very low (at most 25%), it can be assumed that the power required to maintain such a head is around 100 KW.

### 6.4.3 Wellbore heat loss in production tubing

When the water made its way through the reservoir and the heat has risen from 15 °C to 72°C, the water needs to be produced. During the production, the water will lose heat and the system will lose pressure. The heat loss is caused by conduction through the completion and wellbore, while the pressure loss is caused by dissipation of pressure. In order to calculate the heat of the water at the surface, a method proposed by Rolland N. Horne (1979) is used.

#### *6.4.3.1 Horne method*

Based on the well inflow formulas in the model it was calculated that the reservoir can produce 5 $m^3$/hr. In this case a hydrostatic bottomhole pressure of 1.4 MPa is taken into account, without correction for the eventual produced gas. When producing this water through a 0.04 m inner diameter (ID) production tubing, a calculation can be made for the amount of heat that is transferred from the water to the tubing. The calculation starts with the determination of the Nusselt number, which is the ratio between convective and conductive heat transfer:

$$Nu = \frac{hR_{ti}}{k_f} = 0.0265 * Re^{0.8} * Pr^{0.3} \quad (52)$$

Where h, R $_{\text{This}}$ equation is only valid under the following constraints: Re > 10000, 0.7 > Pr > 160, L/D>10. The Prandtl number for water is equal to 7.5. The Reynolds number can be found by the following formula:

$$Re = \frac{\rho v D}{\mu} \quad (53)$$

In this formula $\rho$, $v$, $D$ and $\mu$ are respectively the density, fluid velocity, ID of the tubing and fluid viscosity. From the Nusselt number the heat transfer coefficient can be calculated as follows:

$$h = \frac{Nuk_f}{R_{ti}} \quad (54)$$

In this formula $k_f$is the thermal conductivity of the fluid and $R_{ti}$ is the ID of the tubing. In combination with the conductivities if the different parts of the well completion (See Table 4), the overall heat transfer coefficient of the well can be determined.

Table 4: Input parameters for the total heat transfer coefficient over the production well and completion

| **Completion diameters, m** | | **Condutivity, k [W/mK]** | |
|---|---|---|---|
| OD tubing, Rto | 0.023 | casing | 43.0 |
| ID tubing, Rti | 0.02 | insulation | 0.05 |
| OD Insulation, Rio | 0.053 | cement | 1.0 |
| ID casing, Rci | 0.075 | air, no circulation | 0.024 |
| OD casing, Rco | 0.09 | | |

$$U_T^{-1} = R_{to}\left[\frac{1}{R_{ti}h_f} + \frac{ln\frac{R_{to}}{R_{ti}}}{k_t} + \frac{ln\frac{R_i}{R_{to}}}{k_i} + \frac{1}{R_i h_a} + \frac{ln\frac{R_{co}}{R_{ci}}}{k_c} + \frac{ln\frac{R_d}{R_{co}}}{k_{cem}}\right] \quad (55)$$

The temperature of the produced water at the surface can now be calculated using the following formula:

$$T_1 = (T_o - ay) + aA\left(1 - exp^{\frac{-y}{A}}\right) \quad (56)$$

In this formula $T_1$is the temperature in the tubing, $T_o$is the bottomhole temperature, *a* is the geothermal gradient, *y* is the *y*-coordinate measured from bottomhole depth up to surface and *A* is a group of variables defined as:

$$A = \frac{wc[k+R_{ti}U_t f(t)]}{2\pi k R_{ti} U_t} \quad (57)$$

In this formula *w* is the mass production rate, *c* is the heat capacity of the produced fluid, *k* is the thermal conductivity of the earth, $r_1$ is the inside radius of the tubing, *f(t)* is a dimensionless time function described by Ramey (1962):

$$f(t) = -\ln\left(\frac{R_{ti}}{2\sqrt{\alpha t}}\right) - 0.290 \quad (58)$$

In this formula alpha is the thermal diffusivity of the earth and t is the time after the start of the process. In this formula *t* was chosen to be one month.

#### *6.4.3.2 Results of Horne method*

The following parameters were used to approximate the heat loss from reservoir to surface for the case in the Barendrecht field. It is assumed that the production well consists of an isolated tubing, a layer of air and a cemented casing.

Table 5: Input parameters for the A-function and surface temperature calculation

| Input parameters | | |
|---|---|---|
| Ut | 1.5 | W/m^2*K |
| alpha | 1.03E-06 | m^2/s |
| k,earth | 2.42 | W/mK |
| a | 0.023 | K/m |
| b | 288 | K |

With these parameters a *f(t)* factor of 5.5 and consecutively an *A* factor of $1.6*10^4$ J/K*s was obtained. When applying this *A* factor in equation (56), a surface temperature of 66.8°C is calculated. The model shows that the first 500 years the bottomhole temperature will only drop by three degrees. Therefore no further calculations have to be made for different bottomhole temperatures.

#### *6.4.3.3 Sensitivities*

**Production rate:** By lowering the bottomhole pressure it is possible to increase the production rate in the production well. This can be achieved by installing an electrical submersible pump (ESP) or gas lift on this well. It is difficult to exactly determine the flow rate in the well as a function of bottomhole pressure only. In case the flow rate can be doubled, the surface temperature will be 69.2°C. Results for different flow rates can be seen in Figure 12.

**Tubing radius:** The same kind of analysis is performed in the radius of the tubing size. A smaller tubing size will cause faster flow and therefore less time that the fluid can lose heat. On the other hand, the flow will become more turbulent, therefore the heat transfer process will become more efficient. However, the effect of the higher velocity is bigger than the effect of the transition to laminar flow with increasing wellbore radius. It is assumed that the production from the reservoir is constant, therefore the velocity of the fluid in the tubing will increase with a smaller diameter. The total amount of heat lost is dependent on the heat flow through the casing during production. This heat flow is larger in case of a smaller tubing radius.

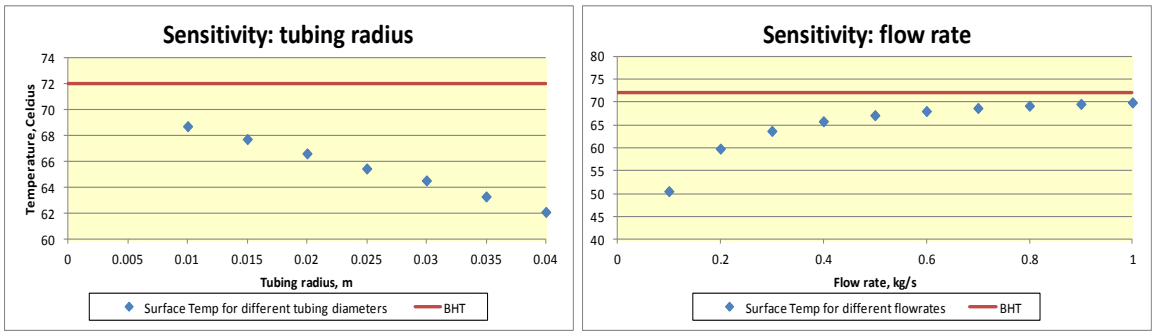


Figure 12: Sensitivity on flow rate and tubing radius

## 6.5 Gas production

The field still possesses around $67*10^6$ $Sm^3$ of natural gas, which will be re-pressurized by the injection of water. At least part of these reserves can be produced after the injection of water has started. The energy that stored in the gas has not been taken into account for this analysis, since that would give a biased view on the exergy of the geothermal plant. Besides the positive effect of the gas, care should be taken that more and heavier surface facilities are necessary in order to produce both water and gas.

## 6.6 Conclusions on exergy

The production of warm water is the only source of energy production. For the flow rate of 5 $m^3$/hr, a surface temperature of 69.7 °C was calculated. So the geothermal energy plant extracted:

$$\Delta Q = \left(T_{prod} - T_{inj}\right) * c_p * \varphi_m = (69.7 - 15) * 4180 * 1.39 = 318\ KW \qquad (59)$$

In order to keep the process going approximately 100 KW are required, resulting in a total exergy of 218 KW. Before the heat can be used, the water first has to go through a heat exchanger. In the heat exchanger also a significant amount of energy will be lost.

So after the 32 years that have been used to saturate the field, the process will create an exergy of around 200 KW for 400 years. The end of the process is marked by the moment that the temperature front breaks through at the producer. It should however be realized that the model is a one dimensional realization of a gas field. There are zones with higher permeability in this field, these zones will show earlier breakthrough of water and eventually of temperature. Section 6.1.4 gives an impression on the effect of permeability on the breakthrough time.

# 7 Conclusions

**Saturation time:** Saturating the Barendrecht gas field with $1.8*10^6$ $m^3$ of water will take approximately 32 years. The low permeability is the main reason that the process takes so long. In case the permeability is doubled to 7 mD, the process would have taken 16 years, instead of 32.

**Permeability:** The permeability of the reservoir is very low, at the average permeability of 3.5 mD only 5 $m^3$/hr can be injected.

**Viscosity:** The model is very sensitive to the viscosity of water. When running the model for a viscosity independent on the reservoir temperature, it takes approximately 50 years instead of 29 years to saturate the field.

**Heat gain:** The inclusion of the heat gain term will disperse the sharp edges of the abrupt heat front. The change of temperature in the reservoir will decrease more gradual compared to the case with no heat gain term. However, for the reservoir thickness used in this study, the temperature will start decreasing at the same distance from the wellbore in both cases.

**Exergy:** The temperature of the produced water is around 69.7 °C, for a flow rate of 1.39 kg/s. This produced water can generate 318 KW, while there is 25 KW needed to produce this amount of heat. The production starts around 29 years later than the injection, so when the geothermal plant is running an exergy of around 200 KW can be obtained.

**Gas Production:** A peak gas production of $0.5 *10^6$ $Sm^3$ per year can be expected. The energy possessed by the gas is not included in the exergy analysis.

**Stimulation:** The permeability problems are found throughout the entire field. Measures to increase the permeability of the field, like hydraulic fracturing or acidizing, are only useful to improve the near wellbore area.

**Heat loss from the wellbore:** in the production well the temperature of the water drops from 72°C to 69.7 °C. An increase in flow rate will cause an increase in surface temperature, while an increase in tubing radius with the same flow rate will cause a decrease in surface temperature.

**Feasibility:** The process will produce a positive exergy of 200 KW after 29 years. Because of the gap between investment and revenues and cheaper alternatives, probably no commercial company would consider exploiting such a project.

# 8 Recommendations

**Field development:** In case the field has better properties for geothermal energy production (higher permeability and higher reservoir temperature), the saturation phase can already be started before the field is abandoned. So if the operator of the field already includes a geothermal afterlife of the field in the development plan, the field still has an economical value after the gas is produced. This can be beneficial for the operator, because he can sell the field without paying for the abandonment costs.

# 9 Nomenclature

| Symbol | Meaning | Unit |
|---|---|---|
| $\phi$ | Porosity | - |
| $\rho_\alpha$ | Density | $kg/m^3$ |
| $K$ | Permeability | $m^2$ |
| $S_\alpha$ | Saturation | - |
| $\mu_\alpha$ | Viscosity | Pa*s |
| $u_\alpha$ | Flow rate | $m^3/s$ |
| $k_{r\alpha}$ | Relative Permeability | - |
| $p$ | Pressure | Pa |
| $\lambda_\alpha$ | Mobility | $m^3s/kg$ |
| $k_{r\alpha e}$ | End Point Relative Permeability | - |
| $S_{w,eff}$ | Effective Saturation | - |
| $c_{p\alpha}$ | Effective Heat Capacity | J/kg*K |
| $T$ | Temperature | K |
| $H_\alpha$ | Enthalpy | J |
| $M$ | Molar Mass | kg |
| $Z$ | Conpressibility Factor | - |
| $R$ | Gas Constant | J/mol*K |
| $\lambda$ | Sorting Factor | - |
| $\Delta\rho_{wg}$ | Density Difference (water-gas) | $kg/m^3$ |
| $f_\alpha$ | Fractional Flow | - |
| $dz$ | Size of a gridcell | m |
| $w$ | Width | m |
| $r_w$ | Wellbore Radius | m |
| $p_{wf}$ | Wellbore Pressure | Pa |
| $t$ | Time | s |
| $u_{tot,i}$ | Total Flow Rate | $m^3/s$ |
| $\Delta Q$ | Energy Difference | $J/m^3$ |
| $k_{ts}$ | Conductivity | W/m*K |
| $\Delta T$ | Temperature Difference | K |
| $\alpha_{ts}$ | Diffusivity | $m^2/K$ |
| $t_k$ | Time at which dT first occurs | s |
| $\Delta S_w$ | Saturation Difference wrt initial Sat. | - |
| $x$ | Length | m |
| $dt$ | time step | s |
| $ds_{max}$ | max allowed change in saturation | - |
| $maxds$ | max observed change in saturation | - |
| $f$ | friction factor | - |
| $D$ | Diameter | m |
| $L$ | Length | m |
| $\Delta\varphi$ | pressure drop | Pa |
| $v$ | velocity | m/s |
| $g$ | gravitational acceleration | $m/s^2$ |
| $z$ | length along a well | m |
| $Nu$ | Nusselt number | - |
| $Re$ | Reynold's number | - |
| $Pr$ | Prandtl's number | - |
| $R_{to}$ | OD tubing | m |
| $R_{ti}$ | ID tubing | m |
| $R_{io}$ | OD insulation | m |
| $R_{ci}$ | ID casing | m |
| $R_{co}$ | OD casing | m |
| $k_f$ | thermal conductivity of fluid | W/m*K |
| $w$ | mass production rate | kg/s |
| $U_T$ | total heat transfer coefficient | $W/m^2*K$ |

| Subscripts | |
|---|---|
| mat | Matrix |
| bulk | Bulk |
| fluid | Pore-fluid |
| w | Water |
| g | Gas |
| s | Solid |
| g,sc | Gas at Standard conditions |
| g,Psc | Gas at Standard conditions |
| c | Capillary |
| i | Spatial Separator |
| n | Temporal Separator |
| pr | Pseudo-reduced |
| pc | Pseudo-critical |
| atm | Atmospheric |
| inj | Injection |
| prod | Production |

# 10 References


580, 1. P. (2004). *Geothermal Energy Recovery from Hydrocarbon Settings: Potential and Challenges.* EGEE 580.

Bertani, R. &. (July 2009). Geothermal Power Generating Plant CO2 Emission Survey. *IGA News (International Geothermal Association) (49)* , 1–3, retrieved 2009-05-13.

Bodvarsson, G. S. (1986). Modeling of geothermal systemsJ. Pet. Tech., 38 (10), 1007-1021. *Journal of Petroleum Technology, 38 (10),* , 1007-1024.

Brill, J. B. (1974). *Two phase flow in Pipes. Textbook for courses on the university of Tulsa.* Tulsa.

Bruining J., E. E. (Consulted: June 2012). Exergy analysis of geothermal energy, a short introduction. *Lecture notes for TuDelft course Geothermics.* Delft.

Carr, N. K. (1954). Viscosity of hydrocarbon gasses under pressure. . *Journal of Petroleum Technology 6 (10), DOI:10.2118/297-G.* , 47-55.

Dempsey, J. (August 1965). Computer routine treats gas viscosity as a variable. *Oil and Gas Journal* , 141-142.

Dobrinsy N. & Nortier, J. (April 2007). *Sedimentology, Petrography and reservoir Quality of Cores 1-3 (Middle Holland Calystone, Holland Greensand and De Lier Member) in well BRT-1.* Panterra Geoconsultants.

Engineeringtoolbox.com. (2011, June). *Density of fluids*. Retrieved from Engineeringtoolbox.com: http://www.engineeringtoolbox.com/fluid-density-temperature-pressure-d_309.html
Engineeringtoolbox.com. (2011, June). *Methane Specific Heat*. Retrieved from Engineeringtoolbox.com: http://www.engineeringtoolbox.com/methane-d_980.html
Engineeringtoolbox.com. (2011, June). *Water-Thermal Properties*. Retrieved from Engineeringtoolbox.com: http://www.engineeringtoolbox.com/water-thermal-properties-d_162.html

Green, R. P. (1997). *Perry's Chemical Engineers' Handbook, 7th Edition.* McGraw Hill.

Masnan, M., Padmanabhan, E., Mokhtar, M., Rajamohan, G., & Prasanna, V. *THERMAL CONDUCTIVITY VALUES OF SOME SANDSTONES AND SHALES FROM THE bELAIT FORMATION.*

Newstead, J. a. (February 2008). *Techniscal Field Development Plan, Barendrecht and Barendrecht-Ziedewij, CO2 Storage, Chapter 7 (Well Integrity & Abandonment Design).* Shell Geostorage BV.

Newstead, J. e. (February 2008). *Technical Field Development Plan, Barendrecht and Barendrecht Ziedewij, CO2 Geostorage, Paragraphs5.2-5.7.* Shell Geostorage B.V.

NLOG.nl. (n.d.). *BRT-01, Boorgatgegevens well*. Retrieved May 2012, from Nlog.nl: http://www.nlog.nl/nlog/requestData/nlogp/allBor/metaData.jsp?tableName=BorLocation&id=106512517

Pollack, H. H. (1993). Heat Flow from the Earth's Interior: Analysis of the Global Data Set. *Rev. Geophys. 30 (3)* , 267–280.

Pone, D. &. (2004). *Geothermal Energy Recovery from Hydrocarbon Settings: Potential and Challenges.* EGEE 580.

Salimi, H. (2010). Geothermal reservoirs, Heat Loss and Heat Gain. *Lecture notes for TuDelft course Geothermics.* Delft.

Tiwari, G. N. (2005). Renewable Energy Resources: Basic Principles and Applications. *Alpha Science Int'l Ltd* , ISBN 1-84265-125-0.

van Bergen F., T. T. (May 2007). *Geochemical consequences of CO2 injection in the Barendrecht and Barendrecht Ziedwij gas fields.* TNO Report 2007-U_R1057/B.

*Horne, R.N., Shinohara, K., (1979)U. of Aukland, Wellbore Heat Loss in Production and Injection Wells, Journal of Petroleum Technology, Volume 31, Number 1*

# Appendix A – Solution techniques

## Saturation Profile

To solve the saturation profile we use an upwind first order scheme for discretisation in space and a forward Euler method for discretisation in time. Using the equations one to four, we achieved a solution for the two phase saturation problem.

$$\int_{i-\frac{1}{2}}^{i+\frac{1}{2}} \frac{\partial}{\partial t}\varphi\left(S_w\rho_w + S_g\rho_g\right)dx + \int_{i-\frac{1}{2}}^{i+\frac{1}{2}} \nabla.\left(u_w\rho_w + u_g\rho_g\right)dx = 0 \quad \text{(A1)}$$

The solution for the first term is:

$$\frac{\partial}{\partial t}\int_{i-\frac{1}{2}}^{i+\frac{1}{2}} \varphi(S_w\rho_w + S_g\rho_g)\,dx = \frac{\partial}{\partial t}\Delta x\varphi(S_w\rho_w + S_w\rho_w)_i = \Delta x\varphi[\frac{(S_w\rho_w+S_w\rho_w)_i^{n+1}-(S_w\rho_w+S_w\rho_w)_i^{n}}{\Delta t}] \quad \text{(A2)}$$

The solution for the second term is:

$$\int_{i-\frac{1}{2}}^{i+\frac{1}{2}} \nabla.\left(u_w\rho_w + u_g\rho_g\right)dx \int \quad = \left(u_w\rho_w + u_g\rho_g\right)_{i+\frac{1}{2}}^{n} - \left(u_w\rho_w + u_g\rho_g\right)_{i-\frac{1}{2}}^{n} = \left(-\frac{k_{rw}}{\mu_w}K\nabla P\rho_w - krg\mu gK\nabla P\rho gi+12n--krw\mu wK\nabla P\rho w-krg\mu gK\nabla P\rho gi-12n=-(((krw\mu w\rho w)in+(krg\mu g\rho g)in)*Kpi+1-pi\Delta x)+(((krw\mu w\rho w)i-1n+(krg\mu g\rho g)i-1n)*Kpi-pi-1\Delta x)\right.$$

(A3)

## Temperature Profile

$$\frac{1}{\Delta t}[\varphi\left(S_w c_{p,w}T\rho_w + S_g c_{p,g}T\rho_g\right)^{n+1} + \left((1-\varphi)cp_s T\rho_s\right)^{n+1}] - [\varphi\left(S_w c_{p,w}T\rho_w + S_g c_{p,g}T\rho_g\right)^{n} + \left((1-\varphi)c_{p,s}T\rho_s\right)^{n}] + \frac{1}{\Delta x}[u_w\rho_w c_{p,w}T + u_g\rho_g c_{p,g}T]_{i+\frac{1}{2}} - \frac{1}{\Delta x}[u_w\rho_w c_{p,w}T + u_g\rho_g c_{p,g}T]_{i-\frac{1}{2}} = 0 \quad \text{(A4)}$$

This equation can be rewritten as:

$$\frac{\varphi}{dt}\left[\rho_w^n c_{p,w}^n((S_wT)^{n+1} - (S_wT)^n) + \rho_g^n c_{p,g}^n\left(\left(S_gT\right)^{n+1} - \left(S_gT\right)^n\right)\right] + \frac{1}{dt}(1-\varphi)c_{p,s}\rho_s(T^{n+1}-T^n) + \frac{1}{\Delta x}[u_w\rho_w c_{p,w}T + u_g\rho_g cp_g T]_{i+\frac{1}{2}} - \frac{1}{\Delta x}[u_w\rho_w c_{p,w}T + u_g\rho_g c_{p,g}T]_{i-\frac{1}{2}} = 0 \quad \text{(A5)}$$

For the saturations of the different phases in the model, equation seven can be used. Using formula seven to start with we obtain the following expression for saturation in a grid model.

$$S_w^{n+1} = S_w^n + \Delta S_w \quad \text{(A6)}$$

$$S_g^{n+1} = 1 - S_w^{n+1} \quad \text{(A7)}$$

$$S_g^{n+1} = 1 - S_w^n - \Delta S_w \quad \text{(A8)}$$

Substituting the equation A8 in equation A5 gives the following:

$$\frac{\varphi}{dt}\left[\rho_w^n c_{p,w}^n((S_w^n + \Delta S_w)T^{n+1} - S_w^nT^n) + \rho_g^n c_{p,g}^n((1-S_w^n-\Delta S_w)T^{n+1} - (1-S_w^n)T^n)\right] + \frac{1}{dt}(1-\varphi)c_{p,s}\rho_s(T^{n+1}-T^n) + \frac{1}{\Delta x}[u_w\rho_w c_{p,w}T + u_g\rho_g c_{p,g}T]_{i+\frac{1}{2}} - \frac{1}{\Delta x}[u_w\rho_w c_{p,w}T + u_g\rho_g c_{p,g}T]_{i-\frac{1}{2}} = 0 \quad \text{(A9)}$$

To achieve a temperature profile we are interested in the change per grid cell in the model. Temperature plus the difference in temperature over the grid cell gives the actual temperature.

$$T^{n+1}\left[\varphi(\rho_w^n c_{p,w}^n(S_w^n+\Delta S_w)+\rho_g^n c_{p,g}^n(1-S_w^n-\Delta S_w)+(1-\varphi)c_{p,s}\rho_s\right]+T^n\left[\varphi(\rho_w^n c_{p,w}^n S_w^n+\right.$$
$$\left.\rho_g^n c_{p,g}^n(1-S_w^n)+(1-\varphi)c_{p,s}\rho_s\right]+\frac{dt}{\Delta x}\left[u_w\rho_w c_{p,w}T+u_g\rho_g c_{p,g}T\right]_{i+\frac{1}{2}}-\frac{dt}{\Delta x}\left[u_w\rho_w c_{p,w}T+u_g\rho_g c_{p,g}T\right]_{i-\frac{1}{2}}=0 \quad \text{(A11)}$$

$$T^{n+1}-T^n=$$
$$\frac{dt}{\Delta x}\left[u_w\rho_w c_{p,w}T+u_g\rho_g c_{p,g}T\right]_{i+\frac{1}{2}}-\frac{dt}{\Delta x}\left[u_w\rho_w c_{p,w}T+u_g\rho_g c_{p,g}T\right]_{i-\frac{1}{2}}-$$
$$T^n\left[\frac{\varphi(\rho_w^n c_{p,w}^n S_w^n+\rho_g^n c_{p,g}^n(1-S_w^n)+(1-\varphi)c_{p,s}\rho_s}{\varphi(\rho_w^n c_{p,w}^n(S_w^n+\Delta S_w)+\rho_g^n c_{p,g}^n(1-S_w^n-\Delta S_w)+(1-\varphi)c_{p,s}\rho_s}\right]-T^n \quad \text{(A12)}$$

# Appendix B – The pressure distribution

In order to develop a pressure distribution in the field which does not cause any formation damage, but which will secure maximum injectivity the IMPEXS numerical scheme was used. From the material balance in Appendix A, the variables a, b, c and r were calculated and later used in a visual basic numerical script.

$$a_n = -\left(\frac{\rho_w^{n-1}\lambda_{rw}^{n-1}}{k} + \frac{\rho_w^n}{\rho_g^n}\frac{\rho_g^{n-1}\lambda_{rg}^{n-1}}{k}\right) \quad \text{(B1)}$$

$$b_n = \frac{\rho_w^n\lambda_{rw}^n}{k} + \frac{\rho_w^{n-1}\lambda_{rw}^{n-1}}{k} + \frac{\rho_w^n\lambda_{rg}^n}{k} + \frac{\rho_w^n}{\rho_g^n}\frac{\rho_g^{n-1}\lambda_{rg}^{n-1}}{k} \quad \text{(B2)}$$

With

$$b_1 = \frac{\rho_w^1(\lambda_{rw}^1+\lambda_{rg}^1)}{k} + \frac{2\pi(\lambda_{rw}^1+\lambda_{rg}^1)\rho_w^1 dz}{\log\left(0{,}208\frac{dz}{r_w}\right)wk} \quad \text{(B3)}$$

$$c_n = -\rho_w^n\frac{(\lambda_{rw}^n+\lambda_{rg}^n)}{k} \quad \text{(B4)}$$

$$r_n = \frac{2\pi(\lambda_{rw}^n+\lambda_{rg}^n)\rho_w^{n-1}dz\ p_{wf}}{\log\left(0{,}208\frac{dz}{r_w}\right)wk} \quad \text{(B5)}$$

The variables are subsequently used in the following script to obtain the desired pressure range.

```
Sub run()
Rem    Cells(7, 8) = 1#
   With Sheets("data")
     .Range("start").Value = 1                    'RESIDUAL OIL SATURATION
     iter = .Range("iterations")                  'RESIDUAL OIL SATURATION
     ncalc = .Range("ncalc")
   End With
   With Application
      .Calculation = xlManual
      .Iteration = True
      .MaxIterations = ncalc
      .MaxChange = 0
   End With
   ActiveWorkbook.PrecisionAsDisplayed = False
   For i = 1 To iter

      a = Worksheets("data").Range("C72 : AY72")
      b = Worksheets("data").Range("C70 : AY70")
      c = Worksheets("data").Range("C71 : AY71")
      r = Worksheets("data").Range("C73 : AY73")
      Sat1 = Worksheets("data").Range("AY60")
      Sat2 = Worksheets("data").Range("AZ60")

      If (Sat2 - Sat1) > 0 Then Exit For

      Dim P(1, 49)
      Dim gam(1, 49)

      bet = b(1, 1)
```

```
        P(1, 1) = r(1, 1) / bet
        For j = 2 To 49
            gam(1, j) = c(1, j - 1) / bet
            bet = b(1, j) - a(1, j) * gam(1, j)
            P(1, j) = (r(1, j) - a(1, j) * P(1, j - 1)) / bet
        Next j
        Worksheets("data").Cells(74, 49 + 2).Value = P(1, 49)
        For k = 49 - 1 To 1 Step -1
            P(1, k) = P(1, k) - gam(1, k + 1) * P(1, k + 1)
            Worksheets("data").Cells(74, k + 2).Value = P(1, k)
        Next k

      ActiveSheet.Calculate

    Next i
End Sub
```

# Appendix C - Input Parameters

| Input Data for 1D Reservoir Model | | | |
|---|---|---|---|
| P_int | 3000000 | [pa] | Reservoir Pressure |
| sinit | 0,15 | [-] | initial water saturaion |
| Height | 30 | [m] | Reservoir Height |
| length | 1000 | [m] | Reservoir Length |
| r_w | 0,1 | [m] | well radius |
| P_wf | 20000000 | [pa] | maximum bottomhole pressure |
| Width | 600 | [m] | Reservoir width |
| theta | 0,00 | [rad] | inj./prod. line with horizontal |
| phi | 0,16 | [-] | porosity |
| k | 3,50E-15 | [m^2] | permeability |
| swc | 0,15 | [-] | connate water |
| sgr | 0,05 | [-] | residual gas saturation |
| kroo | 1 | [-] | end point gas permeability |
| krwo | 1 | [-] | end point water permeability |
| Injection rate | 5 | m^3/hr | injection rate |
| utot | 7,716E-08 | [m/s] | total velocity |
| lambda | 2 | [-] | sorting factor |
| fracdim | 2,5 | [-] | fractal surface dimension |
| rhg | 21,46 | [kg/m^3] | initial density gas |
| rhow | 1000 | [kg/m^3] | initial density water |
| mug | 5,00E-05 | [Pa s] | initial viscosity gas |
| muw | 1,00E-03 | [Pa s] | initial viscosity water |
| g | 9,81 | [m/s^2] | acc. gravity |
| ros | 2650 | [kg/m^3] | reservoir rock density |
| Temp_inj | 293,15 | [K] | Injection temperature |
| Temp_int | 343,15 | [K] | Initial temperature |
| Cpg | 2230 | [J/kg-K] | initial gas heat capacity |
| Cpw | 4190 | [[J/Kg-K] | initial water heat capacity |
| Cps | 1000 | [J/kg-K] | Reservoir heat capacity |
| c | 1,00E-04 | [1/bar] | compressibility factor |

# Appendix D - Permeability Log

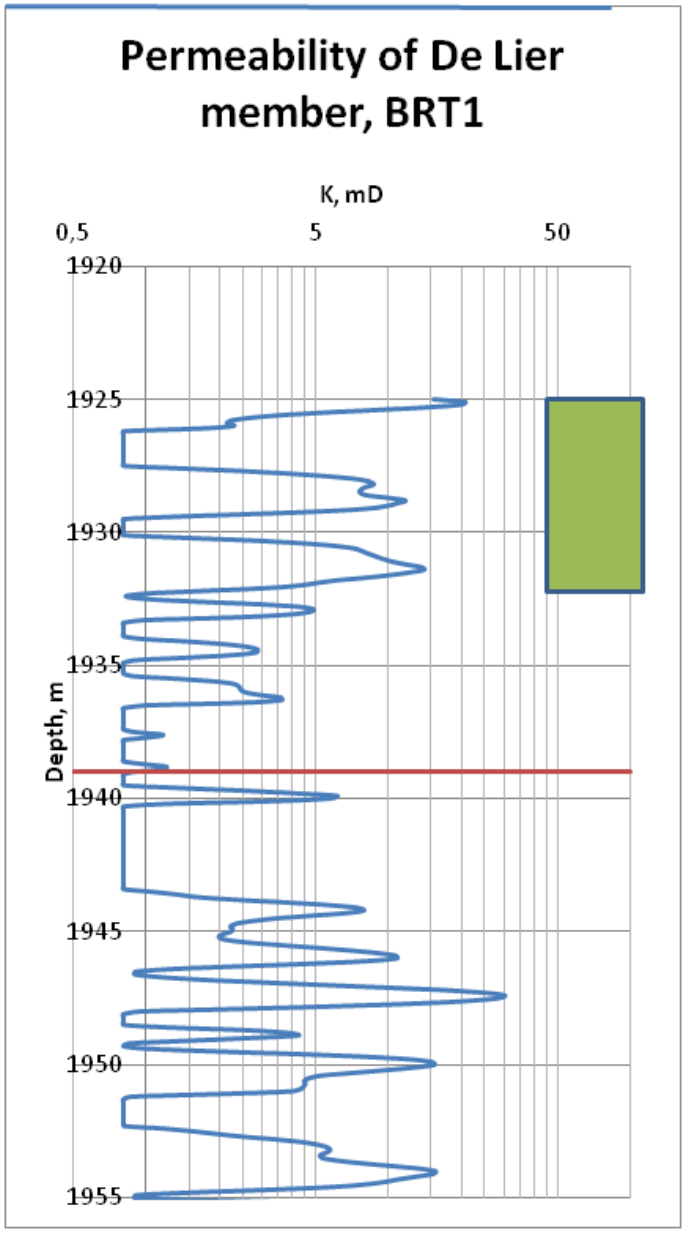


Figure 13: Permeability distribution in the De Lier Member, based on poroperm relation (2). The red line indicates the GOC. The green surface indicates the perforated interval in the well.